Chemosphere 260 (2020) 127211

Contents lists available at ScienceDirect

Chemosphere

journal homepage: www.elsevier.com/locate/chemosphere

Effect of different gases on the sonochemical Cr(VI) reduction in the presence of citric acid

Jorge M. Meichtry [a, b], Lucía Cancelada [a], Hugo Destaillats [c], Marta I. Litter [d, *]

[a] Gerencia Química, Comisión Nacional de Energía Atómica-CONICET, Av. Gral. Paz 1499, B1650, San Martín, Prov. de Buenos Aires, Argentina
[b] Centro de Tecnologías Químicas, Facultad Regional Buenos Aires, Universidad Tecnológica Nacional, Medrano 951, C1179AAQ, CABA, Argentina
[c] Indoor Environment Group, Energy Technologies Area, Lawrence Berkeley National Laboratory, Berkeley, CA, USA
[d] IIIA – Instituto de Investigación e Ingeniería Ambiental-CONICET, Universidad Nacional de General San Martín, Campus Miguelete, Av. 25 de Mayo y Francia, B1650, San Martín, Prov. de Buenos Aires, Argentina

ARTICLE INFO

Article history:
Received 14 November 2019
Received in revised form
2 May 2020
Accepted 23 May 2020
Available online 7 July 2020

Handling Editor: Tsair-Fuh

Keywords:
Cr(VI) sonochemical reduction
Citric acid
H_2O_2 sonochemical formation
KI dosimetry
Effect of different gases

ABSTRACT

The sonochemical (850 kHz) Cr(VI) reduction (0.30 mM, pH 2) in the presence of citric acid (Cit, 2 mM) was analyzed under different working atmospheres: reactor open to air without sparging (ROAWS), and Ar, O_2, air and N_2 sparging. Hydrogen peroxide formation in pure water at pH 2 and KI dosimetry were also measured. Zero-order kinetics was observed in all cases. A complete Cr(VI) reduction after 180 min insonation was obtained with the ROAWS and under Ar, while a lower Cr(VI) reduction efficiency was achieved under the other conditions. The Cr(VI) reduction and H_2O_2 formation rates followed the order ROAWS ≅ Ar > air ≅ O_2 ≫ N_2, while for KI dosimetry the order was ROAWS ≫ O_2 ≅ air > Ar ≫ N_2. This indicates that H_2O_2 formation rate is a better measure of the system reactivity for Cr(VI) reduction. For air, O_2 and N_2, once the sparging was stopped, Cr(VI) reduction rate increased up to approximately the same value obtained for the ROAWS, suggesting that the sparging decreased the generation of reactive species and, thus, the Cr(VI) reduction rate. Nitrate production was measured at low concentrations (micromolar range) in the ROAWS, air and N_2 systems. Formic and acetic acids were detected as Cit degradation products. Reaction mechanisms were proposed. It can be concluded that the best condition for Cr(VI) removal is with the ROAWS because of a higher Cr(VI) reduction rate, no atmosphere control is required, and it is a less expensive system.

© 2020 Elsevier Ltd. All rights reserved.

1. Introduction

Hexavalent chromium (Cr(VI)) is a pollutant present in wastewaters of industrial processes such as leather tanning, industrial painting and electroplating, being considered a priority pollutant due to its acute toxicity, its carcinogenic and mutagenic effects and its high mobility in water. Cr(VI) concentration in drinking water has been regulated in 50 μg L^{-1} by the World Health Organization (2011). Cr(VI) treatment usually involves a reduction step to Cr(III), which is far less mobile and toxic, it is an essential trace metal in human nutrition, and can be easily removed from the solution as a solid after neutralization. (Litter, 2017 and references therein).

In a previous paper, we have analyzed the Cr(VI) reduction (0.3 mM, pH 2, reactor open to the air without sparging (ROAWS)) using ultrasound (850 kHz) in the presence of organic additives such as alcohols and carboxylic acids (Meichtry et al., 2018). Complete Cr(VI) reduction after 180 min was obtained only in the presence of citric acid (Cit) and ethylenediaminetetraacetic acid (EDTA), and Cr(III) complexes with these compounds were detected as final products. A complete mechanism for the Cr(VI) sonochemical reduction has been proposed in that paper, together with a preliminary comparison of the reaction with addition of Cit under air and Ar sparging.

The chemical effect of different gases on ultrasonic transformations has been shown to be a function of different variables such as the nature of the gas bubbles, sparging conditions, pH, ultrasound frequency, ionization potential and water solubility of the gas, and the gas diffusion coefficient (Choi, 2015: Pflieger et al., 2019a and references therein).

On the other hand, hydrogen peroxide formation in sonochemical systems under different working atmospheres has been thoroughly studied (Beckett and Hua, 2001; Pflieger et al., 2015a;

* Corresponding author.
E-mail address: marta.litter@gmail.com (M.I. Litter).

https://doi.org/10.1016/j.chemosphere.2020.127211
0045-6535/© 2020 Elsevier Ltd. All rights reserved.

Dalodière et al., 2016 and references therein). Together with the commonly used Fricke, terephthalate and KI dosimetries, the generation rate of H_2O_2 has also been used as a measure of the generation rate of active species in sonochemical experiments (Nikitenko et al., 2007).

In the present paper, complementary studies of Cr(VI) sonochemical decay in the presence of Cit under different working atmospheres, i.e., ROAWS (no sparging), and under air, O_2, Ar, and N_2 sparging, were performed. Cit was used due to the higher Cr(VI) sonochemical reduction rates obtained before (Meichtry et al., 2018), and because it is a compound usually found in natural and wastewaters (Meichtry et al., 2011). H_2O_2 production in pure water and KI dosimetry were also evaluated, trying to relate these results with the Cr(VI) sonochemical reduction rate. The main object of the research was to determine the best atmospheric working conditions for the Cr(VI) sonochemical reduction.

2. Experimental

2.1. Chemicals and materials

Potassium dichromate was Merck (99.9%), Cit (99%) was Riedel de Häen, and diphenylcarbazide (DPC) was UCB for analysis, dissolved in acetone (Merck, 99.5%). Perchloric acid (70%, Biopack) was used for pH adjustments. All other reagents were of analytical grade and used as received. All solutions and suspensions were prepared with Milli-Q grade water (resistivity = 18 MΩ cm), Osmoion Apema.

2.2. Sonochemical reactor

The sonochemical reactor (60 mm outer diameter, 50 mm height Pyrex tube, 350 mL total volume), ultrasonic transducer (type E/805/T(02), Meinhardt-Ultraschalltechnik, emitting at 850 kHz) and ultrasonic power generator (type K 8-1, Meinhardt-Ultraschalltechnik) were the same used in our previous study (Meichtry et al., 2018). For gas sparging (0.5 L min^{-1}), a diffuser was set in the bottom of the reactor (at 10 mm from the transducer) with a silicone tube (4 mm diameter) entering form the top. An external jacket allowed water recirculation. The temperature of the cooling water in the jacket was 25 °C, and the temperature of the solution was 30 °C, reached 5 min after switching on the power and kept constant throughout the experiment.

The total power input by the transducer into the liquid was 51 ± 2 W L^{-1}, determined by calorimetry using 325 mL of pure water at 25 °C over a period of 3 min with the ROAWS, the water jacket empty and foam insulation in both the reactor and the transducer (Koda et al., 2003; Pflieger et al., 2019b). Potassium iodide oxidation dosimetry with 0.10 M KI at pH 2 was used to evaluate the $HO^{\bullet}$ generation yield in the reactor at 30 °C under the different experimental conditions (Merouani et al., 2010).

2.3. Ultrasonic experiments

The experiments to evaluate Cr(VI) reduction were performed with 325 mL of a 0.30 mM Cr(VI) and 2 mM Cit solution at pH 2 and 30 °C. Changes of pH at the end of all runs were negligible (ΔpH < 0.1). Experiments to assess H_2O_2 production were performed also with 325 mL of water at pH 2 at 30 °C. All experiments were performed at least by duplicate, and the standard deviation among replicates was never higher than 5%. The reported values correspond to the mean of those replicates. The fitting of the experimental points was performed with Origin 8.0 software.

2.4. Analytical determinations

Samples (2 mL) were periodically taken from the reservoir and brought to 10 mL with water to measure Cr(VI), ions and total organic carbon (TOC). Cr(VI) was determined by the DPC method at 540 nm (ASTM, 1999). Ionic chromatography (IC) was used for anions (nitrate, formate and acetate) and ammonium valuation was performed as reported previously (Meichtry et al., 2018). TOC was measured with a Shimadzu 5000-A TOC analyzer in the TOC (total organic carbon) mode. H_2O_2 was determined at 350 nm according to Allen et al. (1952), taking also 2 mL samples from the H_2O_2 experiments. For dissolved oxygen (DO) measurements, a Hach Sension 156 dissolved oxygen meter was used (detection limit, DL, 0.05 mg O_2 L^{-1}).

UV–Vis absorption measurements were performed employing a PG Instruments UV–Vis spectrophotometer, model T80+. UV–Vis absorption spectra were taken in a Hewlett-Packard diode array UV–Vis spectrophotometer, model HP 8453 A.

3. Results and discussion

3.1. Sonochemical reduction of Cr(VI) in the presence of Cit under different working atmospheres

In Fig. 1, results of the sonochemical decay of Cr(VI) (0.30 mM) in the presence of Cit (2 mM) at pH 2 under different atmospheres (ROAWS, air, O_2, N_2 or Ar sparging) are shown.

Under Ar sparging, Cr(VI) decay was almost equal to that with the ROAWS, and was lower under air, O_2 or N_2. When the sparging was arrested (at 180 min in all cases), the reaction rate increased, suggesting that the sparging caused an inhibition effect. In all cases, the evolution of the Cr(VI) concentration could be fitted to a zero-order rate law; the kinetic parameters are shown in Table 1. DO concentrations are also shown in Table 1, and they were almost constant up to 180 min, with the exception of the ROAWS, where a decrease from the initial value from 8.20 mg L^{-1} to 0.57 mg L^{-1} at 180 min was observed (see Fig. S1 in the Supporting Information Section (SI) Appendix A, line 56, page 4); DO evolution for the ROAWS was almost identical for Cr(VI) sonochemical reduction with Cit, for H_2O_2 generation and for KI dosimetry. When the sparging was stopped (at 180 min), DO varied after some time

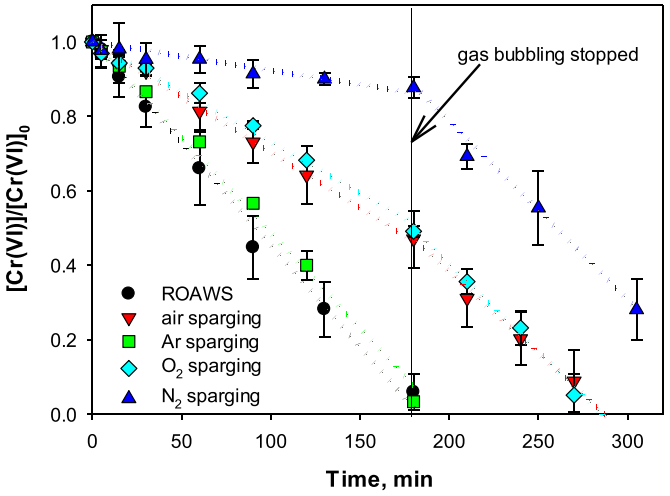

Fig. 1. Sonochemical reduction of Cr(VI) in the presence of Cit under different atmospheres. Conditions: $[Cr(VI)]_0 = 0.30$ mM, $[Cit]_0 = 2.0$ mM, pH 2, $Q_{sparging} = 0.5$ L min^{-1}, $T = 30$ °C. Dotted lines are the zero-order fittings of the experimental points (before and after 180 min).

Table 1
Kinetic parameters for the Cr(VI) decay in the presence of Cit under different atmospheres, extracted from Fig. 1. The concentration of O_2 measured at 180 min is also shown.

Sparging	$k_{Cr(VI)}$ (μM min^{-1}) up to 180 min	R^2	$k'_{Cr(VI)}$ (μM min^{-1}) from 180 min	R^2	O_2 concentration at 180 min (mg L^{-1})
ROAWS	1.64 ± 0.04	0.993	–	0.993	0.56
Ar	1.54 ± 0.03	0.994	–	0.994	<0.05 (below DL)
air	0.89 ± 0.01	0.996	1.32 ± 0.04	0.990	8.2
O_2	0.81 ± 0.02	0.990	1.50 ± 0.05	0.990	>30
N_2	0.23 ± 0.02	0.885	1.43 ± 0.04	0.995	<0.05 (below DL)

under the different conditions. Under O_2, the concentration reached 10 mg L^{-1} after 5 min and 3 mg L^{-1} at 270 min. For air, a gradual decrease from 8.20 mg L^{-1} to 3 mg L^{-1} at 270 min was observed, similarly to that occurred in the ROAWS. Under N_2, the concentration reached 2 mg L^{-1}, 5 min after stopping the sparging.

According to these results, the initial order of reactivity for Cr(VI) reduction, represented by $k_{Cr(VI)}$, is ROAWS ≅ Ar > air ≅ O_2 ≫ N_2, up to the end of the sparging (180 min). Once the sparging was arrested, in the cases of air, O_2 and N_2, Cr(VI) reduction rate ($k'_{Cr(VI)}$) increased, being similar to that in the ROAWS (in the order of the experimental error). The effect of gas sparging on the sonochemical reactions is discussed in Section 3.6.

3.2. Sonochemical H_2O_2 formation in water under different working atmospheres

In Fig. 2, evolution of H_2O_2 at pH 2 under different working conditions is shown. The inset displays the same results but up to 15 min insonation. The evolution of H_2O_2 concentration could be adjusted to a zero-order rate law in all cases.

In Table 2, the kinetic parameters of all curves for H_2O_2 production extracted from Fig. 2 are shown. The parameters are calculated for the whole reaction time (k', $0 \le t \le 180$ min) and for the first 15 min (k'', $0 \le t \le 15$ min). Table 2 shows that k'_{H2O2} varies in the order Ar ≅ ROAWS > O_2 ≅ air ≫ N_2, the same order followed by Cr(VI) removal (Table 1). $HO^\bullet$ generation from KI dosimetry is also indicated in Table 2, with the order ROAWS > air ≅ O_2 > Ar ≫ N_2. This indicates that there is a better correlation of the H_2O_2 generation with the Cr(VI) reduction rate than that obtained from the KI dosimetry. The same order for H_2O_2 generation rate (Ar > O_2 ≅ air > N_2), with very similar values, was found by other authors (e.g., Wakeford et al., 1999). On the other hand, the order for k''_{H2O2} is slightly different from that of k'_{H2O2}, being higher for ROAWS and air. The decrease on H_2O_2 formation rate after a given sonication time can be attributed to: 1) the less effective recombination of $HO^\bullet$ at low pH (Merouani et al., 2010), 2) the decrease in O_2 concentration (for the ROAWS, see Table 1), which decreases the rate of H_2O_2 formation (Pflieger et al., 2015a), and 3) by H_2O_2 consumption at longer times by the sonochemically formed HNO_2 ending in HNO_3 (only relevant when N_2 is present, see later in the SI, lines 25–26, page 2, Scheme S1 Eq. S(7)). It is important to say that the calculation of the $HO^\bullet$ generation yields measured by H_2O_2 generation was performed using k''_{H2O2} values, just to avoid errors due to the decrease on H_2O_2 generation rate.

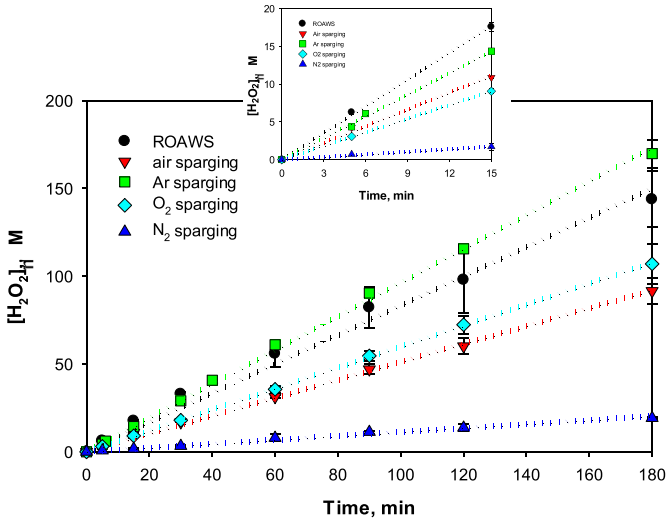

Fig. 2. Sonochemical evolution of H_2O_2. Conditions: pH 2, $Q_{sparging}$ = 0.5 L min^{-1}, T = 30 °C. Dotted lines are the zero-order fittings of the experimental points. Inset: results up to 15 min sonication.

3.3. Mechanisms involved in the sonochemical reduction of Cr(VI) in water

A simplified set of reactions taking place in sonochemical aqueous systems under Ar is shown in Scheme 1. Eqs. (1)–(5) show the main reactions (Adewuyi, 2001 and references therein). The primary reaction is the formation of $H^\bullet$ and $HO^\bullet$ (Eq. (1)); H_2O_2 formation takes place through Eq. (3). In the presence of Cit (a polar, non-volatile additive that remains in the aqueous phase), secondary radicals ($Cit^\bullet$) can be formed in the bulk solution by reaction with $HO^\bullet$ (or $H^\bullet$, not indicated) (Eq. (4), k = 5.0 × 10^7 and 4.0 × 10^5 M^{-1} s^{-1}, respectively for $HO^\bullet$ and $H^\bullet$ (Buxton et al., 1988; Okitsu, 2010; Enomoto and Okitsu, 2015; Meichtry et al., 2018).

Reactions involving hydrogen atoms and hydrogen are minor, and are not included in Scheme 1; this is especially important in the presence of O_2. Regarding hydrated electrons, in our previous paper (Meichtry et al., 2018), it was mentioned that the formation of the highly reducing hydrated electrons has been discarded in sonochemical systems at acid pH (Sehgal et al., 1980; Gutiérrez et al., 1987).

It should be taken into account that, according to Merouani et al. (2015a), up to 25 reactions can take place inside the O_2 and H_2 gas bubbles and 73 reactions are possible inside air and N_2 bubbles.

In the presence of O_2 and under high frequency ultrasound, Scheme 2 shows the simplified reactions taking place.

Atomic oxygen ($O^\bullet$) is sonochemically produced (Eq. (6), Sivasankar and Moholkar, 2009; Pflieger et al., 2015a; Pflieger et al., 2019b). Additionally, all processes involving $H^\bullet$ will be negligible because of the rapid conversion into hydroperoxyl radicals ($HO_2^\bullet$, Eq. (7), k_{10} = 2 × 10^{10} M^{-1} s^{-1}, Al-Sheikhly et al., 1988), making negligible H_2 production. Formation of $HO^\bullet$ and H_2O_2 is increased through Eqs. (8)–(10). According to Hart and Henglein (1985), atomic oxygen atoms ($O^\bullet$) could contribute to H_2O_2 formation only if they were formed in the excited singlet state ($O(^1D)$), but no recent references have been found to discriminate if singlet, triplet, or both $O^\bullet$ species are formed in sonochemical systems. A

[1] All standard reduction potentials vs. SHE.

Table 2
Kinetic parameters extracted from Fig. 2 and $HO^{\bullet}$ generation yield.

Sparging	k'_{H2O2} (μM min^{-1})	R^2	k''_{H2O2}[a] (μM min^{-1})	$G_{HO\bullet} \times 10^9$ (mol J^{-1}) from $k_{H2O2''}$	$G_{HO\bullet} \times 10^9$ (mol J^{-1}) from KI dosimetry	k_{NO3}^{b} (μM min^{-1})	R^{2b}
ROAWS	0.83 ± 0.2	0.999	1.18 ± 0.2	0.76	2.75	0.69	0.998
Ar	0.96 ± 0.1	0.998	0.96 ± 0.2	0.62	1.06		
air	0.51 ± 0.1	0.994	0.74 ± 0.3	0.47	1.31	0.183	0.981
O_2	0.60 ± 0.02	1.000	0.61 ± 0.02	0.39	1.32		
N_2	0.11 ± 0.03	0.992	0.12 ± 0.05	0.075	0.21	0.017	0.954

[a] $R^2 = 1$ for all cases.
[b] calculated for the first 60 min.

$$H_2O +))))) \rightarrow H^{\bullet} + HO^{\bullet} \quad (1)$$

$$H^{\bullet} + H^{\bullet} \rightarrow H_2 \quad (2)$$

$$2\ HO^{\bullet} \rightarrow H_2O_2 \quad (3)$$

$$Cit + HO^{\bullet} \rightarrow Cit^{\bullet} + H_2O \quad (4)$$

$$H^{\bullet} + HO^{\bullet} \rightarrow H_2 + O^{\bullet} \quad (5)$$

Scheme 1. Simplified sonochemical reactions in water under Ar in the presence of Cit.

$$O_2 +))))) \rightarrow 2\ O^{\bullet} \quad (6)$$

$$O_2 + H^{\bullet} \rightarrow HO_2^{\bullet} \quad (7)$$

$$O^{\bullet} + H_2O \rightarrow 2\ HO^{\bullet} \quad (8)$$

$$2\ HO_2^{\bullet} \rightarrow H_2O_2 + O_2 \quad (9)$$

$$O^{\bullet} + H_2O \rightarrow H_2O_2 \quad (10)$$

$$Cit^{\bullet} + O_2 \rightarrow CitOO^{\bullet} \quad 1)$$

Scheme 2. Simplified sonochemical reactions in water in the presence of O_2.

scavenging of reducing radicals $Cit^{\bullet}$ can take place when O_2 is present, yielding peroxy species (Eq. (10), Sostaric et al., 1995). Other ROS and ozone can be formed in sonolytic systems (Adewuyi, 2001), but probably their contribution would be minor, and they are not indicated in Scheme 1. Singlet oxygen ($^1O_2$) sonochemical generation is controversial, depending on the ultrasound frequency (Matsumura et al., 2013); it is suggested to be negligible in the absence of sensitizers (He et al., 2016).

Equations related to the presence of N_2 in sonolytic systems have been moved to the Supporting Information Section, as Section S1, Scheme S1, because they do not have relevant importance on the Cr(VI) reduction. When N_2 is present, it can participate in ultrasonic reactions either by splitting into atomic nitrogen ($N^{\bullet}$) (at high frequency ultrasound, Eq. (S1)) or by reaction with $O^{\bullet}$ (Eq. (S2)). Scheme S1 shows simplified sonochemical reactions in water in the presence of N_2. Under mild oxidizing conditions, N intermediates are oxidized by O_2 and $HO^{\bullet}$, ending in HNO_3 and other less oxidized nitrogenated species after several steps (Adewuyi, 2001, Merouani et al., 2015a; Ouerhani et al., 2015; Pflieger et al., 2019b). The highly reactive oxygen required for nitrite formation from molecular nitrogen would come from the dissociation of O_2 inside the cavitation bubble (Eq. (7), Scheme 2), (Wakeford et al., 1999; Pflieger et al., 2019b). NO is oxidized by $HO^{\bullet}$ (Eq. (S4), Scheme S1), or by O_2 molecules (Eq. (S5)). H_2O_2 can be consumed by HNO_2 ending in HNO_3 (Eq. (S7), Venault et al., 1997). Scheme S1 shows the main equations, valid also under air ($N_2 + O_2$).

Reactions of KI dosimetry have been moved also to the supporting information section, Section S2, Scheme S2, from which Eq. (S8) represents the global reaction:

$$HO^{\bullet} + 2\ I^{-} \rightarrow I_2 + 2\ OH^{-} \quad (S8)$$

In our previous work (Meichtry et al., 2018), it has been determined that the thermal Cr(VI) reduction in the presence of Cit is negligible, indicating that reduction takes place only under ultrasound. Cr(VI) sonochemical reduction can occur according to Scheme 3 by: 1) hydrogen atoms ($H^{\bullet}$); 2) molecular hydrogen; 3) H_2O_2 (Eq. (13).); 4) $HO_2^{\bullet}$ (Eq. (14)); 5) the reducing $Cit^{\bullet}$ radical (Eq. (15)). Scheme 3 shows the mechanism. Reactions 1) and 2), as said before, are minor processes and are not shown in Scheme 3.

Cr(VI) reduction up to Cr(III) by $H^{\bullet}$ attack, although thermodynamically highly feasible processes ($E^0_{(H+/H\bullet)} = -2.3$ V[1] (Breitenkamp et al., 1976)) ($E^0_{(Cr(VI)/Cr(V))} = +0.55$ V; $E^0_{(Cr(V)/Cr(IV))} = +1.34$ V, $E^0_{(Cr(IV)/Cr(III))} = +2.10$ V (Bard et al., 1985)) is not

$$2\ Cr(VI) + 3\ H_2O_2 \rightarrow 2\ Cr(III) + 3\ O_2 + 6\ H^+ \quad (13)$$

$$Cr(VI)/(V)/(IV) + HO_2^\bullet \rightarrow Cr(V)/(IV)/(III) + H^+ + O_2 \quad (14)$$

$$Cr(VI)/(V)/(IV) + Cit^\bullet \rightarrow Cr(V)/(IV)/(III) + Cit_{ox} \quad (15)$$

$$Cr(V)/(IV)/(III) + HO^\bullet \rightarrow Cr(VI)/(V)/(IV) + HO^- \quad (16)$$

$$Cr(V) + H_2O_2 \rightarrow Cr(VI) + HO^\bullet + OH^- \quad (17)$$

$$Cr(VI)/(V)/(IV) + CitOO^\bullet \rightarrow Cr(V)/(IV)/(III) + Cit_{ox} \quad (17)$$

Scheme 3. Proposed mechanism of Cr(VI) reduction by sonochemical reactions.

shown in Scheme 3 because, as said before, reactions with $H^\bullet$ are minor. Reduction of Cr(VI) by H_2 (only significant under Ar and N_2) seems to be small, similarly to the results found by Nagata et al. (1996) for the sonochemical formation of Au nanoparticles. In the present experimental system, the contribution of H_2 can be even lower because it can be blown out by the Ar and N_2 sparging. $HO_2^\bullet$ is a weak reducing radical, and reacts with Cr(VI) with transformation up to Cr(III) (Eq. (14), Al-Sheikhly and McLaughlin, 1991). In the presence of Cr(VI) and in the solution bulk, reaction of $HO_2^\bullet$ through Eq. (14) should be preferred to Eq. (10), considering the rather low second order rate constant for this last reaction ($8.3 \times 10^5\ M^{-1}\ s^{-1}$, Merouani et al., 2015b), and the much higher Cr(VI) concentration than that of the radical. In conclusion, Eq. (13) seems to be the main contributor to Cr(VI) reduction.

The presence of Cit improves the rate and efficiency of Cr(VI) removal (Meichtry et al., 2018), by: i) inhibiting the detrimental Cr(V)/(IV)/(III) reoxidation by oxidative species like $HO^\bullet$ (Eq. (16)), which will attack preferentially Cit, as it is present at high concentration; ii) by generation of $Cit^\bullet$ (Eq. (4)), which contributes to Cr(VI) reduction (Eq. (15)); 3) by stabilization of Cr(V) species (e.g., the monoperoxochromate(V), Meichtry et al., 2018) by complexation.

Although an inhibiting scavenging of reducing radicals $Cit^\bullet$ can take place when O_2 is present (Eq. (15)), Scheme 3), the intermediate peroxy species can still be expected to be able to reduce Cr(VI) (Eq. (18), Scheme 3, Sostaric et al., 1995).

H_2O_2 could also oxidize Cr(V) (Eq. (17)); this reaction generates $HO^\bullet$, and a Fenton type reaction, giving a cyclic Cr(VI)/Cr(V) generation, takes place (Bokare and Choi, 2010; Bokare and Choi, 2011, and references therein). In the absence of Cit, the theoretical Cr(VI) zero-order reduction rate, determined from the H_2O_2 generation rate, is 0.75 μM min^{-1}, very close to the measured value of 0.69 μM min^{-1}; the small difference between these values can be attributed to Eq. (14), indicating that this is a minor reaction (Meichtry et al., 2018).

This mechanism is equivalent to that described for the sonochemical reduction of several inorganic compounds or formation of noble metal particles by ultrasonic irradiation (Nagata et al., 1996; Okitsu, 2010; Pankaj, 2010). Similar mechanisms were proposed for Cr(VI) radiochemical reduction (Al-Sheikhly et al., 1988; Al-Sheikhly and McLaughlin, 1991; Yuan et al., 2006), and for Cr(VI) reduction under discharge and glow discharge plasma (Wang and Jiang, 2008; Ke et al., 2011).

3.4. Products of the sonochemical reduction of Cr(VI) in the presence of Cit under different working atmospheres

Cr(III) formation according to Scheme 3 was confirmed by the band at around 550 nm in the spectra of the final solution of the sonochemical experiments (Fig. 3), when almost complete Cr(VI) reduction was reached. This band corresponds to the Cr(III)-Cit complex (Meichtry et al., 2018); the nature and the amount of the complex at the indicated time is very similar under all conditions, suggesting an analogous Cr(VI) reduction mechanism under all different atmospheres. The difference observed under N_2 sparging can be ascribed to the incomplete Cr(VI) reduction, as clearly appreciated in the inset of Fig. 3, where the 350–500 nm range is enlarged; the peak at 350 nm corresponds to Cr(VI).

As said, Cr(V), Cr(IV) and Cr(III) can be formed according to Scheme 3. Although Cr(III) reduction to Cr(II) ($E^0_{(Cr(III)/Cr(II))} = -0.42$) and even to Cr(0) ($E^0_{(Cr(II)/Cr(0))} = -0.90$ V) could be possible by $H^\bullet$ attack (Bard et al., 1985), Cr(III) is the only product reported in previous works on Cr(VI) sonochemical reduction (Kathiravan and Muthukumar, 2011; Meichtry et al., 2018). In the present work, even under Ar sparging (Fig. 1), where the contribution of $H^\bullet$ to Cr(VI) reduction should be higher due to the absence of O_2, no other product has been detected. However, it is possible that longer reaction times are required to detect the formation of Cr(II) and/or Cr(0).

In the experiments with the ROAWS and under air and N_2 sparging, IC results indicated nitrate formation. Fig. S2 shows the results; NO_3^- evolution was adjusted to a zero-order rate law for N_2 and air up to the end (180 min) and up to 90 min for the ROAWS.

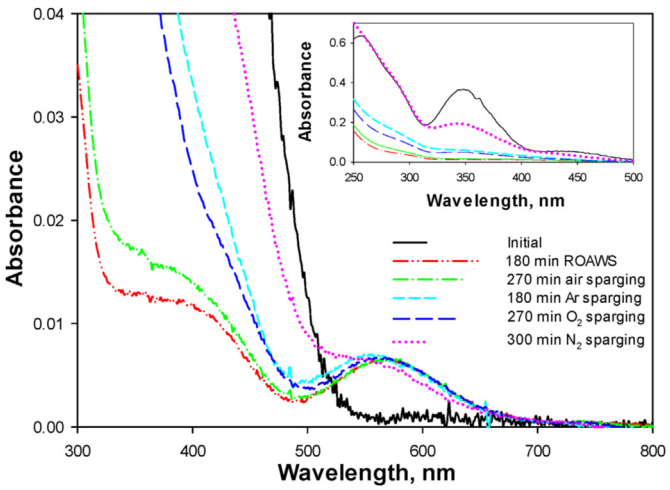

Fig. 3. Spectra of solutions during the sonochemical experiments of Cr(VI) reduction in the presence of Cit under different atmospheres, taken at almost complete Cr(VI) reduction (the time is indicated), with the exception of the reaction under N_2 (taken at 300 min). Conditions: $[Cr(VI)]_0 = 0.30$ mM, [Cit] = 2 mM, pH 2, $T = 30$ °C.

Table 3 indicates the NO_3^- concentrations found at 180 min. The highest concentration was found in the ROAWS, followed by air sparging; under N_2, NO_3^- was formed at very low concentration (in the micromolar range), the same behavior observed for Cr(VI) reduction (Fig. 1), H_2O_2 generation (Fig. 2) and KI dosimetry (Table 2). This indicates that, as long as N_2 is present, NO_3^- values are directly related to the yield of generation of reactive species.

The decrease in the NO_3^- formation rate after 90 min observed in Fig. S2 for the ROAWS can be correlated with the decrease in H_2O_2 formation rate, and ascribed to a decrease in O_2 and N_2 concentrations among other reasons (see section 3.2); although $H^\bullet$ and $Cit^\bullet$ ($E^0(Cit_{ox}/Cit^\bullet) = -1.5$ V, see section S2) could react with the formed NO_3^- ($E^0(NO_3^-/{}^\bullet NO_3^{2-}) = -0.89$ V, Fessenden et al., 2000), the absence of reaction products such as NO_2^- and NH_4^+ indicates that NO_3^- reduction is not taking place in this system.

As mentioned, NO_2^- was never detected, even in the experiments under N_2, probably due to a fast oxidation to NO_3^-. NH_4^+ (or NH_3), another compound that can be formed in sonochemical systems when N_2 is present and O_2 is absent (Sivasankar and Moholkar, 2009; Merouani et al., 2015a; Merouani et al., 2015c) was analyzed as a reaction competing with Cr(VI) reduction, but it was never detected.

The mineralization of Cit measured by TOC was negligible in all cases (<2%). Possible Cit degradation products were analyzed by IC in the ROAWS, under air and under N_2. FA and acetic acid (AA) were the only products detected at rather low concentrations (Table 3). Under Ar, only the final value was measured. The evolution of FA and AA is indicated in Figs. S3 and S4. A linear kinetics was followed for both compounds up to 60 min with very good correlation parameters. With the ROAWS, FA and AA began to decrease after *ca.* 90 and 60 min, respectively. At the working pH, both carboxylic acids are protonated and probably migrate to the gas phase (Hart and Henglein, 1985), where they surely degrade faster than in the liquid phase, as they have to compete with Cit by the $HO^\bullet$. Under the other conditions, the reaction rate is lower and the turning point from where the FA and AA concentrations begin to decrease or stop increasing cannot be seen.

Previous reports of Cit degradation using TiO_2-heterogeneous photocatalysis (pH 2.8) indicate that the most important product was 3-oxoglutaric acid, but acetic (AA) and formic (FA) acids, among other products, were also identified (Meichtry et al., 2011). In the present ultrasonic experiments, FA and AA could be measured in all systems (Table 3), although the concentrations were very low under N_2, in agreement with the low Cr(VI) conversion, KI dosimetry and H_2O_2 generation rate. Under air, the amount of Cit degradation products was similar to those with Ar and with the ROAWS. Cit is degraded to these compounds most probably by $HO^\bullet$ attack. Cit degradation products enhance also the Cr(VI) reduction process as, similarly to Cit, they have the potential of stabilizing Cr(V) species by complexation (Meichtry et al., 2018).

Regarding the effect of the products of Cit degradation on Cr(VI) reduction, as said in the previous paper (Meichtry et al., 2018), FA and AA are inefficient scavengers in sonochemical reactions (Henglein and Kormann, 1985; Findik and Gündüz, 2006, 2007), and they should not inhibit (or to a low extent) H_2O_2 formation; moreover, their concentration was very low compared to that of Cit. In any case, FA would benefit Cr(VI) decay as it scavenges $HO^\bullet$, avoiding Cr(V)/(IV)/(III) reoxidation (Eq. (15)), as it generates the strong reducing $COOH^\bullet$ radical ($E^0 = -1.9$ V) (Eq. (19) Armstrong et al., 2016):

$$HCOOH + HO^\bullet \rightarrow COOH^\bullet + H_2O \quad (19)$$

Table 3
Quantification of products found at 180 min in the sonochemical transformation of Cr(VI) in the presence of Cit under different atmospheres. Conditions: $[Cr(VI)]_0 = 0.30$ mM, [Cit] = 2 mM, pH 2, $T = 30$ °C, sparging flow rate = 0.5 L min^{-1}.

Sparging	$[NO_3^-]$ (μM)	[FA] (μM)	[AA] (μM)
ROAWS	93.5	35	22
Ar	ND	31	15
Air	35.3	37	28
N_2	2.9	10	6
O_2	ND	–	–

ND: not detected.

3.5. Effect of different atmospheres on the sonochemical reduction of Cr(VI) in the presence of Cit and on the H_2O_2 sonolysis

As said in section 3.1, the order of reactivity found for the Cr(VI) sonochemical reduction was ROAWS ≅ Ar > air ≅ O_2 ≫ N_2 (Table 1). Not including the ROAWS, a very different experimental condition due to the absence of sparging (see section 3.6), the decrease in Cr(VI) reduction rate under O_2, air and N_2 compared with the Ar system can be ascribed to a lower generation of radicals, in agreement with the results of H_2O_2 generation rate. Another reason can be that, when O_2 and/or N_2 are present, reactions with $H^\bullet$ will be minor, as atomic hydrogen is consumed by Eq. (6) (Pflieger et al., 2015a); however, the fraction of generated $H^\bullet$ that reacts in liquid phase is usually low (Nagata et al., 1996, 2000) indicate that only 30% of the formed $H^\bullet$ under Ar contributes to Au(III) reduction, despite the high second order kinetic constant for this reaction (5.7×10^9 M^{-1} s^{-1}), which is similar to that of Cr(VI) with $H^\bullet$ (6.9×10^9 M^{-1} s^{-1}, Buxton et al., 1988). Al-Sheikhly et al. (1988) calculated that in the radiolytic reaction of Cr(VI) under O_2, 30% of $H^\bullet$ will react directly with Cr(VI), but in the radiolytic systems, $H^\bullet$ is generated in the aqueous phase, which increases the probability of reaction with Cr(VI).

When pure N_2 is used, besides the low efficiency of generation of radicals (Gielen et al., 2016; Torres-Palma and Serna-Galvis, 2018), the decrease of Cr(VI) reduction could also be ascribed to N_2 fixation by scavenging with $HO^\bullet$ (Wakeford et al., 1999; Sivasankar and Moholkar, 2009), in agreement with the important decrease in H_2O_2 production rate and a lower value of the dosimetry (Table 2). Additionally, the decrease of Cr(VI) decay can be related to the absence of dissolved O_2, responsible in part for the generation of H_2O_2, one of the main contributors to Cr(VI) reduction (Kathiravan and Muthukumar, 2011; Meichtry et al., 2018). As mentioned above, the possible scavenging of $H^\bullet$ by N_2 can be neglected as a reason for the decay in Cr(VI) reduction rate, as it would give NH_4^+ as final product (Sivasankar and Moholkar, 2009; Merouani et al., 2015a; Merouani et al., 2015c), which was not detected.

As said in section 3.2, the order found for $HO^\bullet$ generation calculated from H_2O_2 generation was Ar > O_2 > air > N_2, although other authors reported that the yield of H_2O_2 under O_2 is a little higher than that under Ar (Pflieger et al., 2015a). Merouani et al. (2015c) indicated that the difference can be ascribed to the frequencies used, as for values lower than 515 kHz, the bubble temperature is too high, and a strong consumption of radicals takes place before the full collapse. On the other hand, the $HO^\bullet$ generation calculated from KI dosimetry followed the order air ≅ O_2 > Ar ≫ N_2 (Table 2), with values ≈ 3 times higher than that obtained from H_2O_2 generation when O_2 and/or N_2 are present (ROAWS, O_2, air or N_2 sparging), while under Ar are only 1.7 times higher. This can be explained considering that despite H_2O_2 is generated by different parallel pathways (See Schemes 1 and 2), KI doses not only $HO^\bullet$ migrating to the solution bulk but also other

substances that can oxidize I^-. As said, equations referred to the KI dosimetry are reported in Section S2 (SI), Scheme S2, (Iida et al., 2005; Merouani et al., 2010; Pflieger et al., 2019b). We show the global reaction (Eq. (S8) of Scheme S2, and the rest of Eqs. are in this Scheme S2.

In the presence of H_2O_2, I^- can also be oxidized to I_2 (Eq. (S9)), although this reaction is rather slow in the absence of a catalyst (Hart and Henglein, 1985; Iida et al., 2005). Higher rates of I_3^- formation in acidic solution (as in this work), have been ascribed to the oxidation of I^- by O_2 (Eq. (S10), Merouani et al., 2010), but in the present work, controls indicated that this reaction is negligible. Another possibility could be I^- oxidation by $^1O_2$ (Braathen et al., 1988), but it has been already said that $^1O_2$ sonochemical generation is negligible in the absence of sensitizers (He et al., 2016, see section 3.3). Triplet atomic oxygen ($O(^3P)$) generated by Eq. (6) could additionally oxidize I^- (Eq. (S11), Hart and Henglein, 1985); however, $O(^3P)$ generates $HO^\bullet$ by reaction with H_2O (Pflieger et al., 2015a), and should also contribute to H_2O_2 generation by Eq. (9). At pH 2, I^- can be oxidized by other reactive oxygen species (e.g., $HO_2^\bullet$) that do not generate H_2O_2, or do it with a lower yield. Eq. (9) indicates that 2 $HO_2^\bullet$ gives one H_2O_2, but it can generate up to 3 I_3^- if completely reduced by I^- (Eq. (12)); however, this reaction is also rather slow or null ($k < 10^2\ M^{-1}\ s^{-1}$) (Hart and Henglein, 1985). Finally, when N_2 is present, nitrous acid is formed (Eq. (S4)), which in turn can oxidize I^- (Eq. (S13)), reaction catalyzed by dissolved O_2 (Pflieger et al., 2019b); however, this cannot explain the differences between $HO^\bullet$ yields measured by KI and by H_2O_2 when O_2 is sparged.

Summarizing, the value of KI dosimetry was lower under Ar compared with the other systems containing dissolved O_2 because of the presence of other radicals besides $HO^\bullet$, which increase I^- oxidation, being their effect more significant when O_2 and/or N_2 are present.

Merouani et al. (2015a) report that, under O_2 at 875 kHz, the $HO^\bullet$ production rate is higher than under air, which would lead to a higher H_2O_2 production (Eq. (3)) and, consequently, to a higher Cr(VI) reduction rate. However, Tables 1 and 2 show that $k_{Cr(VI)}$ and $G_{HO^\bullet}$ from the KI dosimetry under O_2 are almost identical to those obtained under air, and that the initial H_2O_2 generation rate ($k"_{H2O2}$, Table 2) is somewhat smaller under O_2 than under air. Therefore, it can be concluded that, in the experimental range of the present O_2 concentrations (8.20–30 mg L^{-1}), no changes in the $HO^\bullet$ generation yield are observed.

The properties of dissolved gases, such as their ratio of specific heats (polytropic index or adiabatic ratio, $\gamma = C_p/C_v$), the solubility in water (S) and, to a lesser extent, the thermal conductivity (Q) determine the hot spot temperature (Beckett and Hua, 2001; Okitsu et al., 2006; Rooze et al., 2013; Gielen et al., 2016; Torres-Palma and Serna-Galvis, 2018), influencing the sonochemical activity. Additionally, recent studies indicate that the gas diffusion coefficient (D) may also play a role (Pflieger et al., 2015b; Pflieger et al., 2019a). The values for γ, Q, S and D of the gases here employed are shown in Table S1. However, there is generally little or no systematic correlation of the sonochemical transformation of chemical species with these properties, this aspect remaining controversial.

Monatomic gases like Ar have typically higher γ than polyatomic gases such as O_2 or N_2, which results in a higher temperature in the bubble at the collapse (Beckett and Hua, 2001; Sivasankar and Moholkar, 2009; Rooze et al., 2013; Merouani et al., 2015b), more energetic implosions and higher generation of radicals. This is confirmed by the observed higher H_2O_2 accumulation when Ar is used (Fig. 2 and Table 2). Similarly, the smaller cavitation effect in air than in Ar, due to the lower γ value, was given as the explanation for the appreciable decrease of the rate of formation of Au nanoparticles under air (Nagata et al., 1996). A similar case is the ROAWS, where the generation of radicals will be higher due to the absence of sparging (see section 3.6), despite the absence of $H^\bullet$ due to the presence of dissolved O_2.

Regarding the effect of gas solubility, systems with higher S will have more gas entering the bubbles, providing more nucleation sites for cavitation and a higher number of bubbles in the medium (Okitsu et al., 2006; Merouani et al., 2015c); however, other authors indicate that a higher S can cushion the collapse (Rooze et al., 2013 and references therein). Nevertheless, in the present case, as Cr(VI) reduction rate, KI dosimetry and H_2O_2 generation rate are almost identical under O_2 and air sparging despite their significant differences in solubility, it can be concluded that S is not a relevant parameter.

A low thermal conductivity has been related to a higher temperature during the bubble collapse and, correspondingly, to a higher radical generation (Beckett and Hua, 2001; Rooze et al., 2013; Gielen et al., 2016). The higher activity under Ar, which has the lower Q, seems to indicate that this parameter is significant; however, Okitsu et al. (2006) has found that the collapse temperature is almost the same for the different noble gases under high frequency ultrasound, despite the large differences in Q, because the process is faster and thus more adiabatic than under low frequency. Therefore, in the present study, the effect of Q could be considered minor.

The gas diffusion coefficient can play a role defining the bubble size, as a high D allows a faster bubble growth in each expansion cycle, enhancing the reactivity of the system (Pflieger et al., 2015b; Pflieger et al., 2019a). However, the highest D value corresponds to N_2 (Table S1), which showed the worst efficiency. Besides, the activity is higher under Ar compared with O_2, although D is the same, and the activity is almost identical under air and O_2, although D is higher for air compared with O_2. Thus, it can be concluded that D is not a relevant parameter in the present study.

Sometimes the overall sonochemical activity is controlled by the nature of the internal bubble chemistry (Rooze et al., 2013; Gielen et al., 2016); i.e., O_2 can compensate the lower bubble temperature (compared with Ar) by the self-decomposition (Merouani et al., 2015c) and by the fast $H^\bullet$ scavenge, preventing any recombination with $HO^\bullet$. This is observed when comparing pure N_2 with O_2 and air bubbling, where the far lower activity under N_2 can be ascribed to the absence of dissolved O_2. Finally, it should be mentioned that although N_2 can generate $N^\bullet$ and NO, which scavenge $HO^\bullet$ (Eq. (S1)-(S4), Ouerhani et al., 201529; Merouani et al., 2015a, 2015c; Gielen et al., 2016; Pflieger et al., 2019b), these are also minor reactions because, as indicated above, the activity under O_2 and air is very similar.

In conclusion, the higher γ would be the main reason for the higher activity under Ar.

3.6. Effect of sparging

In section 3.1, it has been said that, under Ar sparging, Cr(VI) decay was almost equal to that with the ROAWS, and was lower under air, O_2 or N_2 (Fig. 1 and Table 1), the sparging causing a decrease in the reactor performance. Once the gas flow was stopped (at 180 min in all cases), an increase on the Cr(VI) reduction rate was observed (Fig. 1 and Table 1), and it can be considered that all values after stopping the sparging are in the same order within the experimental error and equal to the value with the ROAWS. This is confirmed by the DO concentrations (Table 1), which were almost constant up to 180 min, but when the sparging was stopped, DO reached in all cases values similar to those of the ROAWS (between 2 and 3 mg L^{-1}). H_2O_2, the main Cr(VI) reducing agent, is then generated under all conditions from this O_2 concentration.

The high NO_3^- concentration found in the ROAWS (93.5 μM),

compared with the lower values obtained under air and N_2 (Table 3), reinforces the assumption that the main effect of the sparging is a decrease on the generation rate of reactive species and not the generation of species that might compete with Cr(VI) for the generated H_2O_2, such as NO_2^- (Lukes et al., 2014) that can be oxidized to nitrate, as said before. The effect of the sparging agrees with the decrease on the $HO^\bullet$ generation yield under sparging, measured by both H_2O_2 generation rate and KI dosimetry, which varies in the order ROAWS > air = O_2 > N_2 (Table 2).

The lower activity caused by the sparging can be explained by the coalescence of bubbles generated by the ultrasound, which become sonochemically inactive. Another interpretation is that the sparging would interrupt or destroy the cavitation bubbles, or interfere with the passage of sound waves in the solution, causing a lower cavitational effect (Teo et al., 2001; Gogate et al., 2003; Wood et al., 2017). Our results contrast with those usually found in sonochemical systems, where the sparging increases the efficiency (Gogate et al., 2003; Gogate, 2008; Katekhaye and Gogate, 2011; Pflieger et al., 2015a,b) due to a more homogeneous distribution of the bubbles in the reactive volume and/or to an enhanced number of nuclei for cavitation, although lower ratios of gas flow over treated volume were used by these authors. However, Gogate et al. (2003) also reported that, at higher gas flow/reactor volume ratios, the interference is dominating. In reference Kojima et al.' (2010) a stirrer is used, and gases are not bubbled or sparged, in contrast with our present experiments, where gases are sparged. Although some authors find that sparging or mechanical agitation improves the reaction, it was appreciated in the present paper that bubbling does not causes this enhancement. In another paper of the authors (Kojima et al., 2005), gases were bubbled in the solution, but there the influence of the sparging has been not analyzed.

4. Conclusions

The study of the Cr(VI) sonochemical reduction under different atmospheres is important in order to define the best experimental conditions for the technological use of this system. The ROAWS and Ar sparging gave the best results; reaction under N_2 is the worst condition. The final product of Cr(VI) reduction was, in all cases, Cr(III) in solution forming Cr(III)-Cit complexes. The production of H_2O_2 in the presence of Cit and the identification of Cit degradation products, in addition to formic and acetic acids identified here, will be studied in a next paper. The generation rate of H_2O_2 correlates much better than the KI dosimetry with the Cr(VI) reduction rate, most probably because H_2O_2 is the main species responsible for Cr(VI) reduction. Among the studied sparging gases, Ar proved to be the one that generates the fastest Cr(VI) reduction rate, due to its higher polytropic index, which causes more energetic collapses, generating more reactive species. Although the reaction is favored under Ar, due to the higher rate of generation of reactive species (mainly H_2O_2, but also $H^\bullet$, H_2 and $Cit^\bullet$) among the studies gases, and because NO_3^- is not formed in the process, Ar is an expensive gas, and the control of the working atmosphere implies complex reactors; besides, the sparging gas flow rate used decreased the generation of reactive species. Considering the high rate of Cr(VI) reduction and H_2O_2 generation, and the rather low amount of NO_3^- produced, the ROAWS can be considered the best operative condition.

As commonly found, reactions under N_2 are not convenient, and reactions under O_2 or air are also disfavored, due to the interference caused by the sparging in the generation of reactive species. This contrasts with results of photocatalytic reactions where the presence of O_2 does not reduce the efficiency of Cr(VI) reduction in acidic media (Litter, 2017).

Declaration of competing interest

The authors do not have any conflict of interest about the publication of the manuscript.

Acknowledgements

This work was performed as part of Agencia Nacional de Promoción Científica y Tecnológica PICT-0463, 2015-208 and PICT 3640 projects, and BioCriticalMetals – ERAMIN 2015 grant.

Appendix A. Supplementary data

Supplementary data related to this article can be found at https://doi.org/10.1016/j.chemosphere.2020.127211.

References

Adewuyi, Y.G., 2001. Sonochemistry: environmental science and engineering applications. Ind. Eng. Chem. Res. 40, 4681–4715.
Allen, A.O., Hochanadel, C.J., Ghormley, J.A., Davi, T.W., 1952. Decomposition of water and aqueous solutions under mixed fast neutron and gamma radiation. J. Phys. Chem. 56, 575–586.
Al-Sheikhly, M., Hussmann, M.H., McLaughin, W.L., 1988. Dichromate dosimetry. The effect of acetic acid on the radiolytic reduction yield. Radiat. Phys. Chem. 32, 545–551.
Al-Sheikhly, M., McLaughlin, W.L., 1991. The mechanisms of the reduction reactions of Cr(VI) in the radiolysis of acidic potassium and silver dichromate solutions in the presence or absence of acetic acid. Radiat. Phys. Chem. Int. J. Radiat. Appl. Instrum. Part C 38, 203–211.
Armstrong, D.A., Huie, R.E., Koppenol, W.H., Lymar, S.V., Merényi, G., Neta, P., Ruscic, B., Stanbury, D.M., 2016. Standard Electrode Potentials Involving Radicals in Aqueous Solution: Inorganic Radicals. IUPAC Technical Report 2 PAC-REP-14-05-02 3 4 9, BNL-111793-2016-JA.
ASTM, 1999. Standards D 1687-92.
Bard, A.J., Parsons, R., Jordan, J., 1985. Standard Potentials in Aqueous Solutions. Marcel Dekker Inc., New York.
Beckett, M.A., Hua, I., 2001. Impact of ultrasonic frequency on aqueous sonoluminescence and sonochemistry. J. Phys. Chem. 105, 3796–3802.
Bokare, A.D., Choi, W., 2011. Advanced oxidation process based on the Cr(III)/Cr(VI) redox cycle. Environ. Sci. Technol. 45, 9332–9338.
Bokare, A.D., Choi, W., 2010. Chromate-Induced activation of hydrogen peroxide for oxidative degradation of aqueous organic pollutants. Environ. Sci. Technol. 44, 7232–7237.
Braathen, G., Chou, P.T., Frei, H., 1988. Time-resolved reaction of $O_2(1\Delta)$ with iodide in aqueous solution. J. Phys. Chem. 92, 6610–6615.
Breitenkamp, M., Henglein, A., Lilie, J., 1976. Mechanism of the reduction of lead ions in aqueous solution (a pulse radiolysis study). Ber. Bunsen Ges. 80, 973–979.
Buxton, G.V., Greenstock, C.L., Helman, W.P., Ross, A.B., 1988. Critical review of rate constants for reactions of hydrated electrons, hydrogen atoms and hydroxyl radicals ($^\bullet OH/^\bullet O^-$) in aqueous solution. J. Phys. Chem. Ref. Data 17, 513–886.
Choi, P.-K., Sonoluminescence, in: 2015. F. Grieser, P.-K. Choi, N. Enomoto, H. Harada, K. Okitsu, K. Yasui, Sonochemistry and the Acoustic Bubble https://doi.org/10.1016/B978-0-12-801530-8.00004-9 2015, Elsevier Inc. pp. 85–117.
Dalodière, E., Virot, M., Moisy, P., Nikitenko, S.I., 2016. Effect of ultrasonic frequency on H_2O_2 sonochemical formation rate in aqueous nitric acid solutions in the presence of oxygen. Ultrason. Sonochem. 29, 198–204.
Enomoto, N., Okitsu, K., Application of Ultrasound in Inorganic Synthesis, Chapter 8, Sonochemistry and the Acoustic Bubble. https://doi.org/10.1016/B978-0-12-801530-8.00008-6 2015 Elsevier Inc. 187-206.
Fessenden, R.W., Meisel, D., Camaioni, D.M., 2000. Addition of oxide radical ions (O^-) to nitrite and oxide ions (O_2^-) to nitrogen dioxide. J. Am. Chem. Soc. 122, 3773–3774.
Findik, S., Gündüz, G., 2006. Direct sonication of acetic acid in aqueous solutions. Ultrason. Sonochem. 13, 203–207.
Findik, S., Gündüz, G., 2007. Sonolytic degradation of acetic acid in aqueous solutions. Ultrason. Sonochem. 14, 157–162.
Gielen, B., Marchal, S., Jordens, J., Thomassen, L.C.J., Braeken, L., Van Gerven, T., 2016. Influence of dissolved gases on sonochemistry and sonoluminescence in a flow reactor. Ultrason. Sonochem. 31, 463–472.
Gogate, P.R., 2008. Cavitational reactors for process intensification of chemical processing applications: a critical review. Chem. Eng. Process 47, 515–527.
Gogate, P.R., Mujumdar, S., Pandit, A.B., 2003. Sonochemical reactors for waste water treatment: comparison using formic acid degradation as a model reaction. Adv. Environ. Res. 7, 283–299.
Gutiérrez, M., Henglein, A., Dohrmann, J.K., 1987. H atom reactions in the sonolysis of aqueous solutions. J. Phys. Chem. 91, 6687–6690.
Hart, E.J., Henglein, A., 1985. Free radical and free atom reactions in the sonolysis of

aqueous iodide and formate solutions. J. Phys. Chem. 89, 4342–4347.
He, L.-L., Liu, X.-P., Wang, Y.-X., Wang, Z.-X., Yang, Y.-J., Gao, Y.-P., Wang, X., 2016. Sonochemical degradation of methyl orange in the presence of Bi_2WO_6: effect of operating parameters and the generated reactive oxygen species. Ultrason. Sonochem. 33, 90–98.
Henglein, A., Kormann, C., 1985. Scavenging of OH radicals produced in the sonolysis of water. Int. J. Radiat. Biol. 48, 251–258.
Iida, Y., Yasui, K., Tuziuti, T., Sivakumar, M., 2005. Sonochemistry and its dosimetry. Microchem. J. 80, 159–164.
Katekhaye, S.N., Gogate, P.R., 2011. Intensification of cavitational activity in sonochemical reactors using different additives: efficacy assessment using a model reaction. Chem. Eng. Process 50, 95–103.
Kathiravan, M.N., Muthukumar, K., 2011. Ultrasound mediated reduction of Cr(VI) using sludge obtained during electrocoagulation. Environ. Technol. 32, 1523–1531.
Ke, Z., Huang, Q., Zhang, H., Yu, Z., 2011. Reduction and removal of aqueous Cr(VI) by glow discharge plasma at the gas solution interface. Environ. Sci. Technol. 45, 7841–7847.
Koda, S., Kimura, T., Kondo, T., Mitome, H., 2003. A standard method to calibrate sonochemical efficiency of an individual reaction system. Ultrason. Sonochem. 10, 149–156.
Kojima, Y., Asakura, Y., Sugiyama, G., Koda, S., 2010. The effects of acoustic flow and mechanical flow on the sonochemical efficiency in a rectangular sonochemical reactor. Ultrason. Sonochem. 17, 978–984.
Kojima, Y., Fujita, T., Ona, E.P., Matsuda, H., Koda, S., Tanahashi, N., Asakura, Y., 2005. Effects of dissolved gas species on ultrasonic degradation of (4-chloro-2-methylphenoxy) acetic acid (MCPA) in aqueous solution. Ultrason. Sonochem. 12, 359–365.
Litter, M.I., 2017. Last advances on TiO_2-photocatalytic removal of chromium, uranium and arsenic. Current Opinion in Green Sustain. Chem. 6, 150–158. https://doi.org/10.1016/j.cogsc.2017.04.002.
Lukes, P., Dolezalova, E., Sisrova, I., Clupek, M., 2014. Aqueous-phase chemistry and bactericidal effects from an air discharge plasma in contact with water: evidence for the formation of peroxynitrite through a pseudo-second-order post-discharge reaction of H_2O_2 and HNO_2. Plasma Sources Sci. Technol. 23, 015019.
Matsumura, Y., Iwasawa, A., Kobayashi, T., Kamachi, T., Ozawa, T., Kohno, M., 2013. Detection of high-frequency ultrasound-induced singlet oxygen by the ESR spin-trapping method. Chem. Lett. 42, 1291–1293.
Meichtry, J.M., Quici, N., Mailhot, G., Litter, M.I., 2011. Heterogeneous photocatalytic degradation of citric acid over TiO_2 II. Mechanism of citric acid degradation. Appl. Catal., B 102, 555–562.
Meichtry, J.M., Slodowicz, M., Cancelada, L., Destaillats, H., Litter, M.I., 2018. Sonochemical reduction of Cr(VI) in air in the presence of organic additives: what are the involved mechanistic pathways? Ultrason. Sonochem. 48, 110–117.
Merouani, S., Ferkous, H., Hamdaoui, O., Rezgui, Y., Guemini, M., 2015a. A method for predicting the number of active bubbles in sonochemical reactors. Ultrason. Sonochem. 22, 51–58b.
Merouani, S., Ferkous, H., Hamdaoui, O., Rezgui, Y., Guemini, M., 2015b. New interpretation of the effects of argon-saturating gas toward sonochemical reactions. Ultrason. Sonochem. 23, 37–45c.
Merouani, S., Hamdaoui, O., Rezgui, Y., Guemini, M., 2015c. Sensitivity of free radicals production in acoustically driven bubble to the ultrasonic frequency and nature of dissolved gases. Ultrason. Sonochem. 22, 41–50a.
Nagata, Y., Mizukoshi, Y., Okitsu, K., Maeda, Y., 1996. Sonochemical formation of gold particles in aqueous solution. Radiat. Res. 146, 333–338.
Nagata, Y., Nakagawa, M., Okuno, H., Mizukoshi, Y., Yim, B., Maeda, Y., 2000. Sonochemical degradation of chlorophenols in water. Ultrason. Sonochem. 7, 115–120.
Nikitenko, S.I., Le Naour, C., Moisy, P., 2007. Comparative study of sonochemical reactors with different geometry using thermal and chemical probes. Ultrason. Sonochem. 14, 330–336.
Okitsu, K., 2010. Sonochemical synthesis of metal nanoparticles. In: Pankaj, M. Ashokkumar (Ed.), Theoretical and Experimental Sonochemistry Involving Inorganic Systems. Springer Science & Business Media, Dordrecht, Heidelberg, London, New York, pp. 131–150.
Okitsu, K., Suzuki, T., Takenaka, N., Bandow, H., Nishimura, R., Maeda, Y., 2006. Acoustic multibubble cavitation in water: a new aspect of the effect of a rare gas atmosphere on bubble temperature and its relevance to sonochemistry. J. Phys. Chem. B 110, 20081–20084.
Ouerhani, T., Pflieger, R., Messaoud, W.B., Nikitenko, S.I., 2015. Spectroscopy of sonoluminescence and sonochemistry in water saturated with N_2–Ar mixtures. J. Phys. Chem. B 119, 15885–15891.
Pankaj, 2010. Aqueous inorganic sonochemistry. In: Pankaj, M. Ashokkumar (Ed.), Theoretical and Experimental Sonochemistry Involving Inorganic Systems. Springer Science & Business Media, Dordrecht, Heidelberg, London, New York, pp. 213–271.
Pflieger, R., Chave, T., Vite, G., Jouve, L., Nikitenko, S.I., 2015a. Effect of operational conditions on sonoluminescence and kinetics of H_2O_2 formation during the sonolysis of water in the presence of Ar/O_2 gas mixture. Ultrason. Sonochem. 26, 169–175a.
Pflieger, R., Lee, J., Nikitenko, S.I., Ashokkumar, M., 2015b. Influence of He and Ar flow rates and NaCl concentration on the size distribution of bubbles generated by power ultrasound. J. Phys. Chem. B 119, 12682–12688b.
Pflieger, R., Nikitenko, S.I., Cairós, C., Mettin, R., Sonochemistry, 2019a. In: Pollet, B.G., Ashokkumar, M. (Eds.), Characterization of Cavitation Bubbles and Sonoluminescence, Springer Briefs in Molecular Science, Ultrasound and Sonochemistry. Springer Nature Switzerland AG, ISBN 978-3-030-11717-7, pp. 61–69b. https://doi.org/10.1007/978-3-030-11717-7_2 (eBook).
Pflieger, R., Nikitenko, S.I., Cairós, C., Mettin, R., 2019b. Sonoluminiscence. In: Pollet, B.G., Ashokkumar, M., series (Eds.), Characterization of Cavitation Bubbles and Sonoluminescence, Springer Briefs in Molecular Science, Ultrasound and Sonochemistry. Springer Nature Switzerland AG, ISBN 978-3-030-11717-7, pp. 39–60a. https://doi.org/10.1007/978-3-030-11717-7_2 (eBook).
Rooze, J., Rebrov, E.V., Schouten, J.C., Keurentjes, J.T.F., 2013. Dissolved gas and ultrasonic cavitation – a review. Ultrason. Sonochem. 20, 1–11.
Sehgal, C., Sutherland, R.G., Verrall, R.E., 1980. Cavitation-induced oxidation of aerated aqueous Fe^{2+} solutions in the presence of aliphatic alcohols. J. Phys. Chem. 84, 2920–2922.
Sivasankar, T., Moholkar, V.S., 2009. Mechanistic approach to intensification of sonochemical degradation of phenol. Chem. Eng. J. 149, 57–69.
Sostaric, Z., Mulvaney, P., Grieser, F., 1995. Sonochemical dissolution of MnO_2 colloids. J. Chem. Soc. Faraday. Trans. 91, 2843–2846.
Teo, K.C., Xu, Y., Yang, C., 2001. Sonochemical degradation of halogenated organic compounds. Ultrason. Sonochem. 8, 241–246.
Torres-Palma, R.A., Serna-Galvis, E.A., 2018. Sonolysis. Advanced Oxidation Processes for Wastewater Treatment. Emerging Green Chemical Technology. S.C. Ameta, R. Ameta, J.R.N. Rajasthan Vidyapeeth. Advanced Oxidation Processes for Wastewater Treatment DOI: https://doi.org/10.1016/B978-0-12-810499-6.00007-3 © 2018.
Venault, L., Moisy, P., Nikitenko, S.I., Madic, C., 1997. Kinetics of nitrous acid formation in nitric acid solutions under the effect of power ultrasound. Ultrason. Sonochem. 4, 195–204.
Wakeford, C.A., Blackburn, R., Lickiss, P.D., 1999. Effect of ionic strength on the acoustic generation of nitrite, nitrate and hydrogen peroxide. Ultrason. Sonochem. 6, 141–148 (1999).
Wang, L., Jiang, X.Z., 2008. Plasma-induced reduction of chromium(VI) in an aqueous solution. Environ. Sci. Technol. 42, 8492–8497.
Wood, R.J., Lee, J., Bussemaker, M.J., 2017. A parametric review of sonochemistry: control and augmentation of sonochemical activity in aqueous solutions. Ultrason. Sonochem. 38, 351–370.
World Health Organization, 2011. Guidelines for Drinking-Water Quality, fourth ed. Geneva.
Yuan, S.-J., Zheng, Z., Mu, Y.-Y., Yu, X., Zhao, Y.-F., 2006. Radiation induced reduction of chromium(VI) in aqueous solution by γ-irradiation in a laboratory-scale. J. Environ. Sci. 18, 254–258.